teractions between the model and the tunnel-wall boundary layers" but found the effects to be decreasing with increasing frequency until they were effectively filtered out and "could hardly be detected for $k>0.15$." Thus, the high-frequency results ($\bar{\omega}\geq 0.3$) in Fig. 3 are free from three-dimensional flow-interference effects. However, the lower-frequency results in Fig. 3, as well as the α-ramp data in Figs. 4 and 5, presumably all can have been influenced by three dimensional flow inteference.

Conclusions

It has been shown in the present Note and Ref. 1 how a previously developed quasisteady theory for dynamic stall[2] can be extended to include the transient effects of the "spilled" leading edge vortex. The more important results are as follows.

1) Adding the moving separation point effect to the quasisteady separation value correctly predicts the "spilling" of the leading-edge vortex.

2) The travel of the "spilled" leading-edge vortex over the chord occurs at 55% of freestream speed. Peak pitching moment values occur shortly before the "spilled" vortex leaves the trailing edge, and peak normal force occurs when the vortex is at 70% chord.

3) By the use of Polhamus' leading-edge suction analogy, a simple means is provided for prediction of the loads induced by the "spilled" vortex.

The present analytic method correctly predicts the large "spilled" vortex effect measured in high-amplitude oscillations in pitch. Furthermore, the developed analytic means predict the very nonlinear characteristics for rampwise change of angle of attack observed by Ham et al. (when due consideration is taken of the experimental accuracy). These results all indicate that the present analytic method could be applied to predict the nonlinear, nonharmonic unsteady characteristics of a helicopter blade passing through the stall region.

References

[1]Ericsson, L. E. and Reding, J. P., " 'Spilled' Leading Edge Vortex Effects on Dynamic Stall Characteristics," *Journal of Aircraft,* Vol. 13, April 1976, pp. 313-315.

[2]Ericsson L. E. and Reding, J. P., "Dynamic Stall Analysis in Light of Recent Numerical and Experimental Results," *Journal of Aircraft,* Vol. 13, April 1976, pp. 248-255; also AIAA Paper 75-26.

[3]McCroskey, W. J., "Recent Developments in Dynamic Stall," *Symposium on Unsteady Aerodynamics,* University of Arizona, Tucson, Ariz., March 18-20, 1975.

[4]McCroskey, W. J., Carr, L. W., and McAllister, K. W., "Dynamic Stall Experiments on Oscillating Airfoils," *AIAA Journal,* Vol. 14, Jan. 1976, pp. 57-63.

[5]Ham, N. D. and Garelick, M. S., "Dynamic Stall Considerations in Helicopter Rotors," *American Helicopter Society Journal,* Vol. 13, April 1968, pp. 44-55.

[6]Ericsson, L. E. and Reding, J. P., "Dynamic Stall Reconsiderations," *Proceedings AIAA 3rd Atmospheric Flight Mechanics Conference,* Arlington, Texas, June 7-9, 1976, pp. 70-78.

[7]Jacobs, E. N. and Sherman, A., "Airfoil Section Characteristics as Affected by Variations in the Reynolds Number," NACA TR 586, 1937.

[8]Ericsson, L. E. and Reding, J. P., "Unsteady Airfoil Stall, Review and Extension," *Journal of Aircraft,* Vol. 8, Aug. 1971, pp. 609-616.

[9]Von Kármán, T. and Sears, W. R., "Airfoil Theory for Non-Uniform Motion," *Journal of the Aeronautical Sciences,* Vol. 5, Aug. 1938, pp. 379-390.

[10]Ericsson, L. E. and Reding, J. P., "Dynamic Stall Stimulation Problems," *Journal of Aircraft,* Vol.8, July 1971, pp. 579-583.

[11]Moss, G. F. and Murdin, P. M., "Two-Dimensional Low-Speed Tunnel Tests on the NACA 0012 Section Including Measurements Made During Pitch Oscillations at the Stall," Aeronautical Research Council, Great Britain, C P 1145, 1971.

Bodies of Revolution with Wavy Afterbodies at Large Incidences

V. S. Holla* and B. S. Varambally†
Indian Institute of Science, Bangalore, India

Introduction

ROCKET and missile shapes, during flight, usually deform both longitudinally and circumferentially because of the aerodynamic loads acting on the flexible structure. A knowledge of the aerodynamic forces and moments on these deformed shapes is important from both stability as well as aeroelastic viewpoints. At low incidence one can use the well-known slender-body theory to calculate the normal force and pitching moment, and it may very well turn out that changes in these quantities caused by body deformation are negligibly small. However, at large incidences, because of viscous crossflow separation, the effect of body deformation on the normal force, moment, and center of pressure may not be negligible. In the present Note the effect of body deformation in the form of longitudinal waviness along the afterbody on the normal force, moment, and center of pressure is considered under the conditions of laminar flow at subcritical Reynolds numbers.

Analysis

The well-known simple method to estimate the total normal force C_N, pitching moment C_M coefficients on slender bodies at large incidence is to superimpose the results from slender-body theory for linear parts (C_{N1}, C_{M1}) and a proper crossflow theory for nonlinear parts (C_{N2}, C_{M2}) of C_N and C_M. Allen's[1] crossflow drag concept as extended by Kelly[2] (using the impulsive flow analogy) is used here to calculate the C_{N2} and C_{M2}. Using Sarpakaya's (Fig. 6, Ref. 3) experimental results, the crossflow drag variation along the body is represented by

$$C_{D_c}(x)=\sum_{1}^{6} a_n\left\{\frac{x\tan\alpha}{r(x)}\right\}^n \tag{1}$$

The a_n's, obtained by a curve-fitting procedure, are given by: $a_1=0.4632$, $a_2=-0.48295\times10^{-1}$, $a_3=0.20405\times10^{-2}$, $a_4=-0.20392\times10^{-4}$, $a_5=-0.23214\times10^{-6}$, and $a_6=0.707475\times10^{-8}$. Next, the cross-sectional radius of a body with power law ogival nose and wavy afterbody shape can be written as

$$r(x)=R_B(x/H)^p \qquad 0\leq x\leq H$$

$$r(x)=R_B+\delta\sin[(x-H)N\pi/(L-H)] \qquad H\leq x\leq L \tag{2}$$

where N is the number of half-waves and δ is the amplitude (Fig. 1). For this wavy body, the linear parts of normal force and moment coefficients C_{N1W} and C_{M1W} are obtained, using the slender-body theory of Munk and Ward, to give

$$C_{N1W}=\sin2\alpha\cdot\cos(\alpha/2) \tag{3}$$

$$C_{M1W}=[V-S_B(L-X_m)]\sin2\alpha\cos(\alpha/2)/S_B\cdot D_B \tag{4}$$

where V, the volume of the body, is given by

$$V=[\pi R_B^2H/(2p+1)]+\pi R_B^2(L-H)+\pi\delta^2(L-H)/2$$
$$+2\delta R_B(L-H)(1-\cos N\pi)/N \tag{5}$$

Received Oct. 21, 1976; revision received Jan. 5, 1977.

Index categories: Aerodynamics; LV/M Aerodynamics; Jets, Wakes, and Viscid-Inviscid Flow Interactions.

*Assistant Professor.

†Aerodynamics Engineer, VSSC Trivendrum, India.

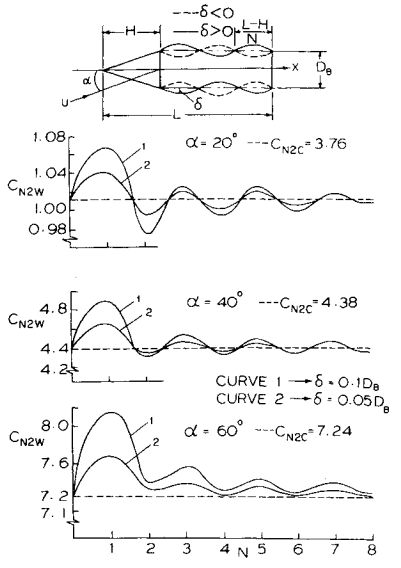

Fig. 1 C_{N2W} vs N at $\alpha = 20°, 40°$, and $60°$.

The nonlinear parts C_{N2W} and C_{M2W} are given by[2]

$$C_{N2W} = \frac{2\eta \sin^2\alpha}{S_B} \int_0^L C_{D_c}(x) r(x) \mathrm{d}x \tag{6}$$

$$C_{M2W} = \frac{2\eta \sin^2\alpha}{S_B D_B} \int_0^L C_{D_c}(x) r(x) (X_m - x) \mathrm{d}x \tag{7}$$

Substituting for $C_{D_c}(x)$ and $r(x)$ from Eqs. (1) and (2) in Eqs. (6) and (7) we get, on simplification

$$C_{N2W} = \frac{2\eta \sin^2\alpha}{S_B} \left[a_1 \tan\alpha \frac{L^2}{2} + \sum_{n=2}^{6} \frac{a_n \tan^n\alpha H^{n+1}}{R_B^{n-1}[(n+1) - p(n-1)]} + \sum_{n=2}^{6} a_n \tan^n\alpha \int_H^L \frac{x^n}{[r(x)]^{n-1}} \mathrm{d}x \right] \tag{8}$$

$$C_{M2W} = \left(\frac{X_m C_{N1W}}{D_B}\right) - 2\eta \sin^2\alpha \left[a_1 \tan\alpha \frac{L^3}{3} + \sum_{n=2}^{6} a_n \tan^n\alpha \frac{H^{n+2}}{R_B^{n-1}} [(n+2) - p(n-1)] + \sum_{n=2}^{6} a_n \tan^n\alpha \int_H^L \{x^{n+1}/[(r(x)]^{n-1}\} \mathrm{d}x \right] \Big/ S_B D_B \tag{9}$$

where η is the scaling factor multiplying $C_{D_c}(x)$ to account for finite length of the body. Finally, the distance of center of pressure in terms of D_B from the nose is given by

$$\bar{X}_{C.P.W.} = X_m/D_B - [(C_{M1W} + C_{M2W})/(C_{N1W} + C_{N2W}) D_B] \tag{10}$$

Results and Discussion

On the basis of the good agreement between the results estimated using the present method and experimental results for the test case of a body with ogival nose and cylindrical body (for which experimental results for C_N and $\bar{X}_{C.P.}$ are available in Fig. 3a of Ref. 4), the numerical results were obtained for the wavy configurations with the following results: $L = 10D_B$, $H = 3D_B$; $\delta = 0.05D_B$, $0.1D_B$; $N = 1$ to 8, $p = 1$, $X_m = L$. In Figs. 1-3 variations in C_{N2W}, C_{M2W}, and $\bar{X}_{C.P.}$, respectively, with N are shown at $\alpha = 20°, 40°$, and $60°$. In each case the corresponding value for the cone cylinder is indicated. C_{N1W} is not affected by N; the changes in C_{M1W} with N are not shown here, but are accounted for in calculating $\bar{X}_{C.P.W.}$

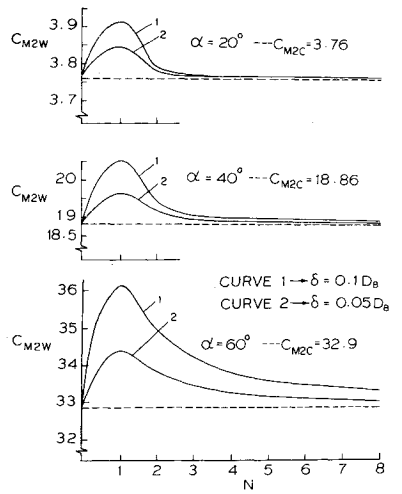

Fig. 2 C_{M2W} vs N at $\alpha = 20°, 40°$, and $60°$.

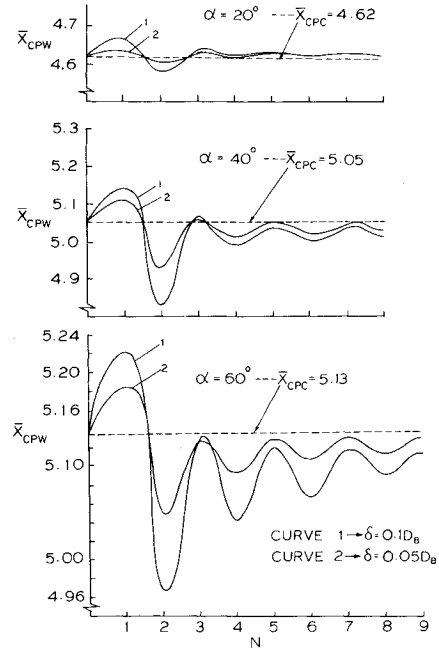

Fig. 3 $\bar{X}_{C.P.}$ vs N at $\alpha = 20°, 40°$, and $60°$.

From Fig. 1 it is seen that $\Delta C_{N2W} = [C_{N2W} - C_{N2C}]$ is maximum for $N = 1$ and decreases with increase in N. At a given incidence the ΔC_{N2W} becomes zero for all $N \geq N_1(\alpha)$. From Fig. 2, we see that, with further increase in N, $\Delta C_{M2W} = [C_{M2W} - C_{M2C}]$ also eventually will become zero for all $N \geq N_2(\alpha)$ (e.g., it was found at $\alpha = 10°$, $\Delta C_{N2W} = 0$ for $N \geq N_1(\alpha) = 7$ and $\Delta C_{M2W} = 0$ for $N \geq N_2(\alpha) = 8$). This means that at values of $N < N_1(\alpha)$, waviness alters the total nonlinear normal force as well as its distribution along the body, whereas in the range $N_1(\alpha) \leq N < N_2(\alpha)$, it only alters the distribution. Finally, at values of $N \geq N_2(\alpha)$, the flow does not seem to distinguish between the wavy and nonwavy bodies. Another interesting feature is that at a given odd value of $N = \bar{N}$, ΔC_{N2W} is greater than the ΔC_{N2W} at the preceding and succeeding even values of $N = (\bar{N} - 1)$ and $(\bar{N} + 1)$ (Fig. 1). Further, the ΔC_{N2W} at these even N's can even be negative (e.g., at 20° and 40°) at lower incidences. However, with further increase in incidence, all of the wavy bodies have a positive ΔC_{N2W} at all values of $\alpha \geq \alpha_L$ ($\alpha_L = 47°$ for the present configuration), the value of which depends on the parameters L/D, N, p, and δ. With regard to variation in

C_{M2W} (Fig. 2), we see that at all incidences it is maximum when $N=1$ and decreases rapidly to C_{M2C} with increase in N. Finally, from Fig. 3, it is seen that at all incidences $\bar{X}_{C.P.}$ moves forward (toward the nose) when N is even and backward (toward the base) when N is odd, with the maximum backward shift occurring at $N=1$ and maximum forward shift occurring at $N=2$. But, at lower incidence (e.g., at $\alpha=20°$), the $\bar{X}_{C.P.W.}>\bar{X}_{C.P.C.}$ for all N except $N=2$, whereas at higher incidences $\bar{X}_{C.P.W.}<\bar{X}_{C.P.C.}$ for all $N>1$, i.e., $\bar{X}_{C.P.W.}$ shifts toward the nose because of the finite number of waves along the body, before ultimately tending to $\bar{X}_{C.P.C.}$ as N becomes very large.

Conclusions

The results discussed so far pertain to the case when the first half-wave near the shoulder is convex ($\delta>0$). However, the results for $\delta<0$, when plotted as in Figs. 1-3, will be almost mirror images of the corresponding curves for $\delta>0$. Hence, the increase or decrease in C_{N2W}, C_{M2W}, and $\bar{X}_{C.P.}$ will depend primarily on whether the first half-wave is convex or concave. The present study shows that the development of one or two half-waves causes significant changes in normal force, moment, and center of pressure, when the wave amplitude is of the order of 5 to 10% of D_B. However, the development of large numbers of half-waves is not at all critical from a stability point of view.

References

[1]Allen, H. J. and Parkins, E. W., "A Study of the Effects of Viscosity on Flow over Slender Bodies of Revolution," NACA Rept. 1048, 1951.

[2]Kelly, H. R., "The Estimation of Normal Force, Drag, and Pitch wing Moment Coefficients for Blunt Based Bodies of Revolution at Large Angles of Attack," *Journal of Aeronautical Sciences*, Vol. 21, Aug. 1954, p. 549.

[3]Sarpakaya, T., "Separated Flow about Lifting Bodies and Impulsive Flow about Cylinders," *AIAA Journal*, Vol. 4, March 1966, p. 414.

[4]Jorgenson, L. H., "Experimental Aerodynamic Characteristics for Bodies of Elliptic Cross Section at Angles of Attack from 0° to 58° and Mach Numbers from 0.6 to 2.0," NASA TMX 3129, Feb. 1975.

Drag of Circular Cylinders at Transonic Mach Numbers

John M. Macha*
Texas A&M University, College Station, Texas

Introduction

THE static longitudinal forces and moments of aircraft and missiles at high angles of attack can be predicted by semiempirical techniques which combine the lift derived from potential flow theory with a force due to the separation of the viscous crossflow normal to the vehicle longitudinal axis.[1] Evaluation of the viscous term requires an experimentally determined crossflow drag coefficient which may be a function of both Mach number and Reynolds number. Since many vehicle cross sections are at least approximately circular, drag coefficients of circular cylinders over the Mach number range of low-subsonic to supersonic are critical to the semiempirical approach.

The results of numerous wind-tunnel experiments which have measured the drag of bluff cylindrical cross sections are available in the literature (see, for instance, the bibliography in Ref. 1). Most of those tests were conducted at either low subsonic Mach numbers where compressibility and tunnel wall interference can be ignored and/or corrected for, or in supersonic flow where wall interference again becomes tolerable. The results of these experiments have shown that the flow around bluff cylinders at Mach numbers less than about 0.25 is dominated by Reynolds number effects, having either a subcritical or supercritical value of the drag coefficient. At Mach numbers greater than about 2.0 the available data indicate little or no dependence on Reynolds number, and the drag coefficients approach the modified Newtonian value for hypersonic flow.

Data on cylinder drag through the transonic speed range are few. The reported wind-tunnel measurements at high subsonic Mach numbers are influenced to an unknown extent by wall interference.[2,3] An earlier flight test program produced drag coefficients at Mach numbers from 0.5 to 1.3, but with no method to separate the effects of Mach number and Reynolds number.[4] To fill this gap in the data, a wind-tunnel investigation has been conducted specifically to determine drag coefficients for circular cylinders at transonic Mach numbers. Additional data and a detailed account of the experimental procedures are available in Ref. 5.

Experiment and Results

The experiment was carried out in the 0.6-×0.6-m transonic wind tunnel of the NASA Ames Research Center. This facility has an operating Reynolds number range of 0.5×10^6 to 8.7×10^6 per ft, with Mach number independently variable from 0.2 to 1.4.

Stainless steel circular cylinders of four different diameters were tested. Each cylinder completely spanned the test section horizontally, midway between the upper and lower slotted walls. Blockage ratios of cylinder diameter to tunnel height were 0.031, 0.042, 0.062, and 0.084. Surface pressures were measured at nine orifices equally spaced around the circumference. The cylinders were rotated in increments of three degrees to provide a pressure distribution adequate to compute the drag. A drag coefficient C_D based on the projected model area normal to the flow was computed for

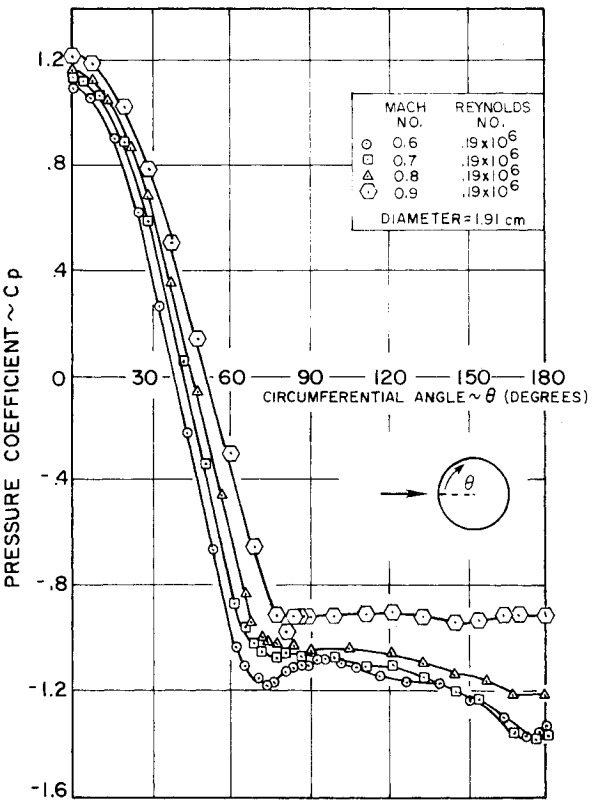

Fig. 1 Surface pressure distributions around a circular cylinder at high subsonic Mach numbers.

Received Feb. 24, 1977.
Index categories: Transonic Flow; LV/M Aerodynamics.
*Graduate Student, Department of Aerospace Engineering.